Cathepsin B-degradable, NIR-responsive nanoparticulate platform for target-specific cancer therapy

Cathepsin B-degradable, NIR-responsive nanoparticulate platform for target-specific cancer therapy

2017 Nanotechnology 28 055101

(http://iopscience.iop.org/0957-4484/28/5/055101)

OPEN ACCESS
IOP Publishing
Nanotechnology

Nanotechnology **28** (2017) 055101 (12pp)
doi:10.1088/1361-6528/28/5/055101

Cathepsin B-degradable, NIR-responsive nanoparticulate platform for target-specific cancer therapy

Sam P Tarassoli[1], Alejandra Martinez de Pinillos Bayona[1], Hayley Pye[1], C Alexander Mosse[1], John F Callan[2], Alexander MacRobert[1], Anthony P McHale[2] and Nikolitsa Nomikou[1,3]

[1] Division of Surgery & Interventional Science, University College London, Royal Free Hospital, Pond Street, NW3 2PF, London, UK
[2] Department of Pharmacy and Pharmaceutical Sciences, University of Ulster, Cromore Road, BT52 1SA, Coleraine, UK

E-mail: n.nomikou@ucl.ac.uk

Received 29 July 2016, revised 10 October 2016
Accepted for publication 7 November 2016
Published 28 December 2016

Abstract

Stimuli-responsive anticancer formulations can promote drug release and activation within the target tumour, facilitate cellular uptake, as well as improve the therapeutic efficacy of drugs and reduce off-target effects. In the present work, indocyanine green (ICG)-containing polyglutamate (PGA) nanoparticles were developed and characterized. Digestion of nanoparticles with cathepsin B, a matrix metalloproteinase overexpressed in the microenvironment of advanced tumours, decreased particle size and increased ICG cellular uptake. Incorporation of ICG in PGA nanoparticles provided the NIR-absorbing agent with time-dependent altered optical properties in the presence of cathepsin B. Having minimal dark toxicity, the formulation exhibited significant cytotoxicity upon NIR exposure. Combined use of the formulation with saporin, a ribosome-inactivating protein, resulted in synergistically enhanced cytotoxicity attributed to the photo-induced release of saporin from endo/lysosomes. The results suggest that this therapeutic approach can offer significant therapeutic benefit in the treatment of superficial malignancies, such as head and neck tumours.

S Online supplementary data available from stacks.iop.org/NANO/28/055101/mmedia

Keywords: indocyanine green, polyglutamate, cathepsin B, near infra-red, laser cancer treatment

(Some figures may appear in colour only in the online journal)

1. Introduction

Nanotechnology has significantly contributed in improving drug bioavailability and therapeutic index in cancer therapy. Nanoparticulate formulations have been developed that, apart from serving as drug carriers, have the attribute to respond to endogenous, disease-associated stimuli or externally applied stimuli [1]. Responsiveness to these stimuli can offer spatiotemporal treatment control by promoting site-specific accumulation, drug release and/or activation in or around target lesions.

In cancer, disease-specific stimulation can be provoked by the well-known distinctive characteristics of the tumour microenvironment, such as the acidic pH [2], the enhanced permeability and retention (EPR) effect [3], the abundance of proteolytic enzymes [4], hypoxia [5] and the overexpression of particular cell membrane receptors [6]. Among these, the

[3] Author to whom any correspondence should be addressed.

EPR effect involves atypical and leaky vasculature, as well as poor lymphatic drainage that promote nanoparticle accumulation and retention in tumours [3]. The tumour microenvironment also contains upregulated proteolytic enzymes, such as matrix metalloproteinases, that are required for cancer progression. These endogenous tumour-specific characteristics provide valuable tools for the design of formulations that will only be activated in the tumour microenvironment. Polyglutamate (PGA) is among the biodegradable polymeric molecules that have been successfully used in drug delivery systems for cancer, mainly as PGA-drug conjugates. PGA can be digested by cathepsin B, which is a lysosomal protease in normal cells and tissues [7]. In malignant tumours, the expression of cathepsin B is highly upregulated and the enzyme is secreted into the extracellular environment [8]. The concept of using PGA as a carrier for anticancer agents is based on the observation that drugs appear to be inactive while bound onto PGA chains and they elicit their cytotoxic action once the polymer backbone is digested within the tumour microenvironment [9]. PGA-based formulations have been developed that have significantly enhanced the efficacy of agents, such as camptothecin and paclitaxel, not only by promoting tumour-specific cytotoxicity but also by improving their solubility in blood following systemic administration [1, 10]. For instance, clinical studies on paclitaxel polyglumex, a PGA-paclitaxel conjugate, have demonstrated that this drug formulation is preferentially trapped in the tumour microenvironment allowing the tumour to be exposed to significantly higher chemotherapeutic concentrations than those in off-target tissues [7, 9, 11].

Externally-applied stimuli that can be employed in drug delivery and drug activation for cancer include light, ultrasound, magnetic fields and heat. Among these, light has been successfully employed as a stimulus for the locoregional ablation of superficial lesions, such as skin, as well as head and neck cancers. Apart from laser-induced interstitial thermotherapy that uses light as the sole heat-producing source, laser light is often used with light-sensitive drugs, known as photosensitizers, to kill cancer cells in a treatment known as photodynamic therapy (PDT) [12]. In PDT, light in combination with a photosensitizer, triggers the production of cytotoxic reactive oxygen species that lead to the non-thermal ablation of lesions. It has been shown that amphiphilic photosensitizers can be integrated in the cytoplasmic membrane, subsequently translocate to the endo/lysosomal membranes so that the latter become light-sensitive [13]. Sensitization of the latter can result in the release of components that are compartmentalized in endocytic vesicles when exposed to light. This treatment modality, known as photochemical internalization (PCI), is a novel technology for release of endocytosed agents, such as ribosome-inactivating proteins, therapeutic nucleic acid or bleomycin, into the cytosol prior to their deactivation by lysosomal enzymes [14]. A photothermal approach has also been developed for triggering cytosolic release of agents via endosome disruption, in a similar manner as PCI. The photothermally-triggered cytosolic drug delivery approach involved the inclusion of agents that absorb light for the production of heat, which can induce endo/lysosomal disruption and subsequently enhance chemotherapy [15, 16]. Among the photoresponsive agents used for the light-based therapeutic modalities described above, those that absorb light in the near-infrared (NIR) region of the electromagnetic spectrum have received considerable attention. The advantage of using NIR light (650–900 nm wavelength) in treatment is that it provides deeper tissue penetration when compared with light of lower wavelengths [17]. In addition, the presence of an NIR-absorbing agent within the tumour mass can lower the threshold of the energy required to achieve an ablative effect locally [18].

Indocyanine green (ICG) is a NIR-absorbing dye approved by the US FDA and has been used clinically as a diagnostic agent in angiography. More recently, the use of ICG for tumour imaging, hyperthemic cancer ablation and laser-induced drug release has gained increasing attention. When exposed to NIR laser light, ICG can convert the absorbed energy into heat due to internal conversion [19]. This results in local hyperthermia with subsequent ablative effects in tumours [20]. Moreover, a number of studies have demonstrated the non-hyperthemic cytotoxic effects of ICG under NIR irradiation. These effects include the photo- and sonosensitizing activity of ICG, as well as the induction of PCI of chemotherapeutic agents on the basis of the amphiphilic nature of the molecule. In our own studies, we have demonstrated the cytotoxic and antitumour effect of intratumorally-injected ICG, in combination with laser light and low-intensity ultrasound [21]. The photo- and sonosensitizing effects of ICG, triggered by light and ultrasound irradiation, have been attributed to mitochondrial destruction that leads to the build-up of intracellular cytotoxic free radicals and subsequent cell death.

A number of different aspects limit the applicability of ICG in laser-based cancer ablation. This limitation has been attributed to the instability of ICG in aqueous solutions and the high affinity of this molecule for plasma proteins after intravenous injection, followed by rapid hepatic elimination from blood circulation [22]. These characteristics result in poor biodistribution of this agent after systemic administration and a very short half-life of only about 2–4 min [23]. Efforts have been made to overcome these limitations mainly by physical encapsulation of ICG into delivery systems for improving the efficacy of this agent in cancer imaging and therapy [20, 24, 25].

In this study, we describe novel PGA-based nanoparticles carrying ICG for NIR-based treatment of head and neck cancers. The nanoparticulate formulation developed herein is intended to improve the optical properties of ICG for systemic administration, improve tumour accumulation and facilitate improved cellular uptake of the light-responsive agent. The use of the formulation to elicit stimulus-responsive cytotoxic effects and also to improve cellular uptake of saporin, a ribosome-inactivating protein, upon NIR irradiation is evaluated using an *in vitro* target.

2. Methods

2.1. Cell culture

SCC-9, a human squamous carcinoma of the tongue cell line, was obtained from Sigma, UK. The cell line was maintained in DMEM/Ham's F-12 tissue culture medium supplemented with 2 mM glutamine (GibcoBRL,UK), 0.5 mM sodium pyruvate, 10% v/v fetal bovine serum (Life Technologies, UK) and 0.2 μg hydrocortisone (Sigma, UK) at 37 °C in a 5% CO_2 humidified atmosphere. When required, single cell suspensions were prepared by treating cell monolayers with a 0.05% w/v solution of trypsin containing 0.02% w/v EDTA in phosphate-buffered saline (PBS).

2.2. PGA digestion with cathepsin-B

PGA (0.1 mg ml^{-1}) was incubated with cathepsin B (from human placenta; Sigma-Aldrich, UK) (0.6 units ml^{-1}) in PBS for 3 days, in an orbital incubator, at 37 °C. 10 μl aliquots were obtained from the incubating mixture every 24 h. Samples were stored at −20 °C and were treated with reducing SDS loading buffer prior to gradient SDS/PAGE. Following electrophoresis, gels were stained with coomassie blue for 24 h for exposing the ladder bands and subsequently, with alcian blue (BDH Chemicals, UK) for visualizing PGA [26].

2.3. Preparation of ICG-PGA nanoparticles

Nanoparticles were prepared using a modification of the protocol suggested by Zia *et al* [27]. Briefly, 5 mg of poly-l-glutamic acid sodium salt (PGA) (M_W: 50–100 kDa; Sigma-Aldrich, UK) and 5 mg of ICG (Sigma Aldrich, UK) were dissolved in 10 ml of dimethyl sulfoxide (DMSO). This was added drop-wise to a poly(vinyl alcohol) solution (10 mg in 5 ml H_2O) (M_W: 30–70 kDa; Sigma-Aldrich, UK) under constant stirring. The resulting mixture was stirred at room temperature for 1 h and was then dialysed (MWCO: 8 kDa) against deionised water, for 24 h. The dialysed suspension was centrifuged at 38 000 g for 1 h using a Beckman OptimaTM L-80 Ultracentrifuge. The pellet was washed twice with deionised water and was then suspended in 2 ml of water. The precipitated nanoparticles were then probe-sonicated for 3 min, followed by further dialysis against water, for 12 h, to remove any free ICG. The dialysed solution was then filtered using a micro syringe filter (0.22 μm). The suspension was snap-frozen and freeze dried for 48 h.

2.4. Nanoparticle characterization and the effect of digestion with cathepsin B

The methods employed to characterize the nanoparticles in terms of size, surface charge and morphology are described in detail in the supplementary material. In order to determine the effect of cathepsin B on nanoparticle degradation, an enzymatic digestion assay was set up followed by size-exclusion filtration through a MWCO 300 kDa membrane (supplementary material).

For time-depended absorbance and fluorescence emission characterization, PBS solutions/suspensions (pH 7.4) containing free ICG, or ICG nanoparticles in the absence (ICGNP) or the presence (d.ICGNP) of cathepsin B (0.6 units ml^{-1}) were stored in an orbital incubator at 37 °C, protected from light, for 3 days. The equivalent ICG concentration in all systems was 6 μg ml (7.8 μM). Absorption and fluorescence emission spectra of these systems were acquired at predetermined times. The excitation wavelength of 740 nm was used to obtain the fluorescence spectra. For the afore-mentioned experiments, spectra and fluorescence intensities were obtained using a CLARIOstar® High Performance Monochromator Multimode microplate reader (BMG LABTECH, UK).

2.5. Cellular uptake of nanoparticles

In order to study the cellular uptake of the ICG-containing formulation and the effect of cathepsin B digestion on uptake, SCC-9 cells were added to individual wells of 96-well plates at a concentration of 9×10^3 cells/well. 24 h later, each ICG formulation (free ICG, ICGNP, d.ICGNP) was added in serum-containing growth medium in each well at a final ICG concentration of 3 μM. The effect of saporin on nanoparticle cellular uptake was also examined. Saporin was added at a final concentration of 40 nM. All systems were incubated at 37 °C in a 5% CO_2 humidified atmosphere for 24 h. The growth medium was removed and cell monolayers were washed with medium. 50 μl of DAPI solution (300 nM) was added to each well and plates were examined using the microplate reader. Further details on the experimental set-up are provided in the supplementary material.

2.6. NIR-laser treatment of cells

In order to examine the effect of laser light on cells treated with ICG nanoparticles, saporin, or the combination thereof, SCC-9 cells were seeded in 96-well plates at a concentration of 9×10^3 cells/well. After 24 h, saporin and/or each ICG-containing formulation (free ICG, ICGNP, d.ICGNP) were added to the serum-containing growth medium in each well at a final ICG concentration of 3 μM. Saporin was added at a final concentration of 40 nM. All systems were incubated at 3 °C in a 5% CO_2 humidified atmosphere for 24 h. The medium was removed, and cell monolayers were washed and refilled with fresh medium. Systems were irradiated with light, through a CUT-END Model OTO00 optical fibre (Medlight, Switzerland), at 805 nm and 150 mW cm^{-2}, for 5 min (45 J cm^{-2} total energy), using a BIOMED 25 (Biomed Ltd, UK) laser. Treatments we performed at room temperature (22 °C). The actual irradiating power density that the target samples were exposed to (150 W cm^{-2}) was calibrated each time using a Gentec TPM-300 laser power metre. Treated cells were further incubated for 24 h, before examination of cell viability using a bioluminescence-based assay. The thermal effects of NIR laser irradiation in the cell treatment was measured with a thermocouple. The photo-induced agent internalization with rhodamine-dextran as a surrogate for

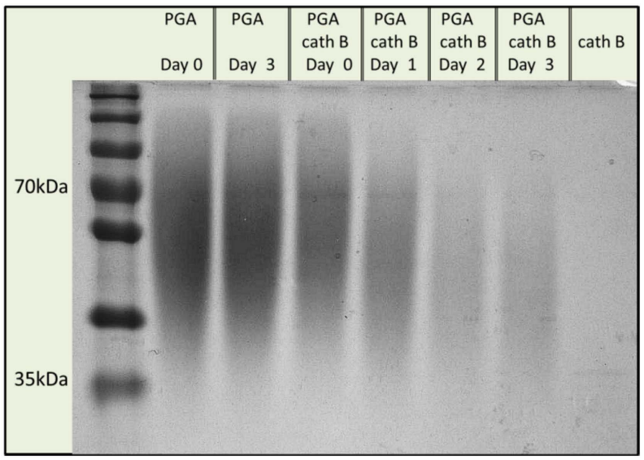

Figure 1. SDS-PAGE electrophoresis of PGA incubated in the absence or the presence of cathepsin B (cath B) over 72 h.

saporin was examined using microscopy. These methods are described in detail in the supplementary material.

2.7. Statistical analysis

Results are shown as mean or mean ± standard deviation. Unless otherwise stated, two-way ANOVA with Bonferroni post-test was performed to evaluate significance among multiple groups in GraphPad Prism version 5.01. Herein, a single asterisk (*) indicates $P < 0.05$, double asterisk (**) indicates $P < 0.01$ and triple asterisk (***) indicates $P < 0.001$.

3. Results and discussion

3.1. PGA digestion with cathepsin-B

PGA is a polypeptide that is cleaved by cathepsin B over-expressed in the tumour microenvironment and this phenomenon has previously been used for improving the tumour uptake of agents in clinically available formulations. In order to assess the effect of cathepsin B on PGA, the latter was incubated in the presence or the absence of the proteolytic enzyme at 37 °C over the course of 3 days. Samples acquired every 24 h were subjected to gel electrophoresis and the image of the resolving gel is shown in figure 1. PGA samples incubated in the absence of cathepsin B showed a smear-like band extending from the highest (170 kDa) to the lowest (35 kDa) molecular weights. The profile of the smear-like band, in terms of breadth and intensity remained unchanged even after incubation for 3 days in the absence of cathepsin B. However, in the presence of cathepsin B, the smear-like band became less intense with digestion time and shifted towards lower molecular weights. In addition to verifying that the PGA remained stable for 3 days in the absence of cathepsin B, the SDS-PAGE analytical system also proved useful in verifying that our preparation of PGA was also sensitive to cathepsin B.

3.2. Nanoparticle characterization and the effect of digestion with cathepsin B

For the preparation of the PGA-based nanoparticles containing ICG a self-assembly method was employed and this resulted in an encapsulation efficiency of 8 ± 1.60% ($n = 3$). The mean hydrodynamic diameter of the undigested nanoparticles as determined using DLS was 113 ± 1.78 nm ($n = 3$) and images from scanning electron microscopy (SEM) showed nanoparticles with globular morphology (figure 2(a)). The surface potential of the particles was −7 ± 1.3 mV ($n = 3$). Enzymatic digestion of the nanoparticles with cathepsin B for 3 days resulted in measurable globular particles with mean hydrodynamic diameter 56 ± 1.22 nm ($n = 3$), which shows a 50% decrease in average size. The digestion-induced decrease in size was further confirmed with SEM analysis (figure 2(b)). Enzymatic digestion also results in smaller structures in the form of PGA complexes with ICG or free ICG (figure 3(a)), as confirmed by results from the experiments using size-exclusion filtration (figure 3(b)). Here ICG-containing nanoparticles were digested with cathepsin B and both these and undigested samples were subjected to size exclusion filtration using a 300 kDa cut-off membrane. Filtrates were examined using fluorescence spectroscopy for ICG and those from the digested formulation showed a 48% increase in fluorescence ($p = 0.002$, independent t-test) when compared with the undigested sample (figure 3(b)). The latter demonstrates that, apart from nanoparticle size reduction detected by DLS, cathepsin B digestion results in the formation of smaller ICG-PGA complexes and/or free ICG (figure 3(a)).

In order to more fully characterize the optical properties of the nanoparticles optical profiles of free ICG, ICG nanoparticles (ICGNP) and ICG nanoparticles in the presence of cathepsin B (d.ICGNP) were compared by examining their absorbance and fluorescence spectra in PBS solutions/suspensions over a period of 4 days. Figure 4 displays the absorbance (figure 4(a)) and fluorescence (figure 4(b)) spectra of free ICG, ICGNP and d.ICGNP, incubated at 37 °C, over the course of 4 days. Initially (Day 0), the sample of free ICG showed the characteristic ICG absorbance profile in PBS with peak maximum at 774 nm. The absorption profile of the nanoparticulate formulation displayed a broad peak, extending over a wider NIR wavelength range. The broad peak resolves after 24 h revealing a peak at 774 nm, which suggests release of free ICG from the nanoparticles. A similar phenomenon has been observed in previous studies employing ICG-containing nanoparticulate formulations, such as liposomes and emulsions [28, 29]. The sharper peak at 774 nm that appeared in the case of the digested sample, suggests an improved rate of ICG release when compared with the undigested system. The newly formed peak that appeared at 888 nm confirmed the complexation of ICG with PGA to form nanoparticles with a subsequent significant red shift, probably associated with the formation of so called J-aggregate [30]. The appearance of an absorbance peak at significantly higher wavelengths than that of the free agent has been observed previously in the case of NIR-absorbing

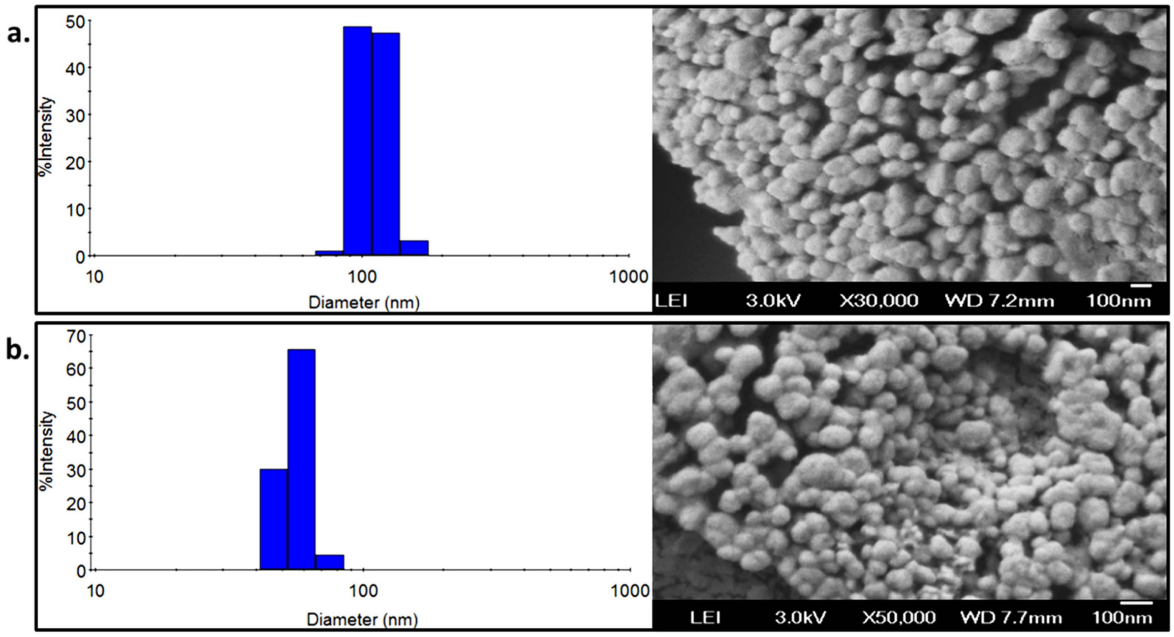

Figure 2. Size distribution using DLS and SEM images of the undigested (a) and enzyme-digested (b) nanoparticles.

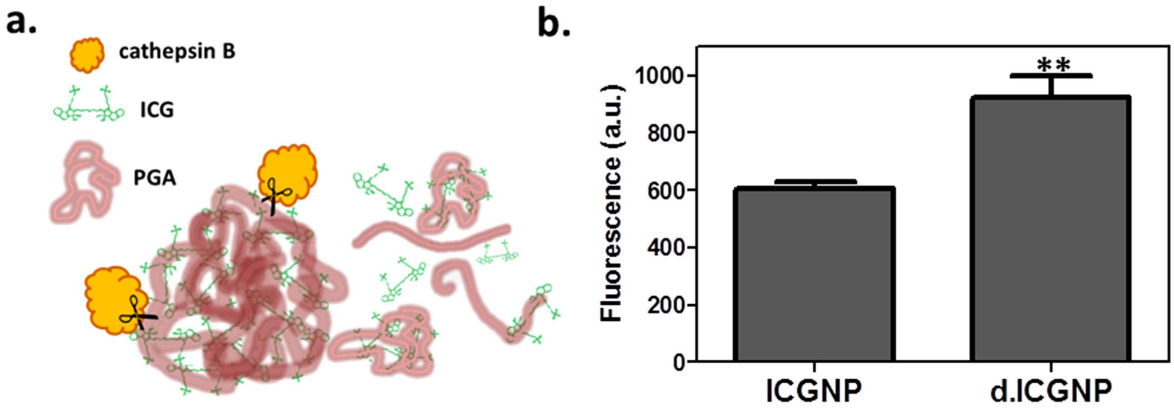

Figure 3. (a) Schematic illustration of nanoparticle enzymatic digestion, with subsequent formation of smaller particles and release of free ICG, and (b) fluorescence emission of filtrates from size-exclusion filtration of the undigested (ICGNP) and digested (d.ICGNP) nanoparticles ($n = 3$).

cyanine dyes in complexation with protein molecules [31]. In that study it was found that the absorbance peak that appeared at higher wavelengths as a result of the formation of cyanine-protein complexes was soon replaced by a Soret absorption band at wavelengths lower than that of the free cyanine. In the current study, the newly formed peak at 888 nm that corresponds to the absorbance of the ICG nanoparticulate complexes with PGA was sustained even after the absorbance of the free ICG declined over the period of 4 days. In addition, no blue shift in the absorbance spectra of the formulation was observed over time. The attribute of the formulation to absorb lower energy light than the free agent will be the subject of further investigations and it could offer potential for the treatment of deeper lesions. The absorbance spectra in figure 4(a) also confirmed a considerable difference in stability between the free ICG and the ICG incorporated in nanoparticles. The maximum absorbance at 888 nm after 24 h decreased in a time-dependent manner at 37 °C either due to release of ICG and subsequent destabilization of the agent in aqueous solution or due to slow destabilization of the agent within the nanoparticles. Degradation of ICG in aqueous media is caused by saturation of the double bonds in the conjugated molecule, with subsequent decrease of both the absorbance and fluorescence [32]. A number of studies have reported the development of ICG-carrying nanoparticulate formulations for improving ICG stability at 37 °C in aqueous media. A study by Yan & Qiu demonstrated that incorporation of ICG in the hydrophobic environment of polymeric micelles provided the molecule with chemical stability over a period of 10 d [20]. Although the hydrophilic nature of the formulation described in the current study did not provide the level of ICG stability reported in previous studies, from a practical perspective the spectra demonstrated adequate stability to allow a 3-day window for repeated treatment if required in a clinical environment.

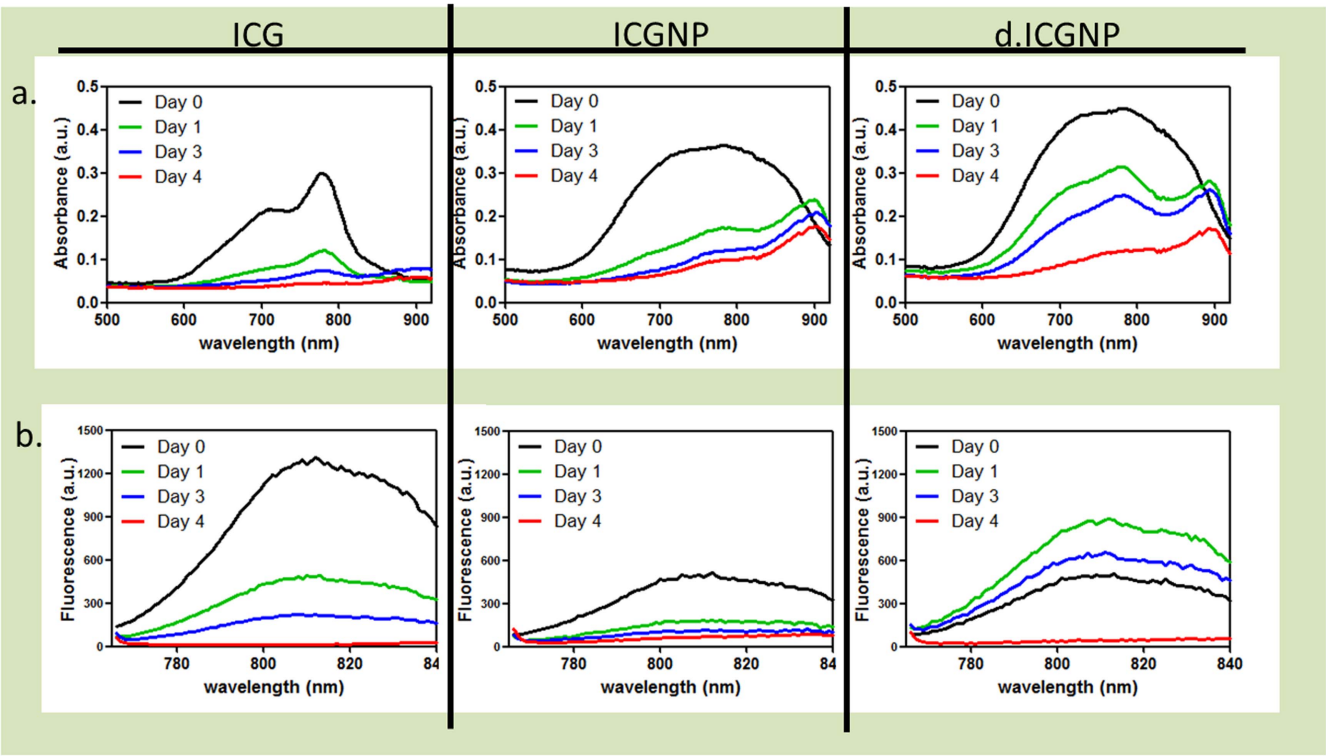

Figure 4. Time-dependent evolution of the absorbance (a) and fluorescence (b) spectra of free ICG (ICG), nanoparticles (ICGNP) and nanoparticles in the presence of cathepsin B (d.ICGNP), incubated at 37 °C in the time course of 4 days.

Fluorescence spectra showed that incorporation of ICG in the nanoparticulate formulation resulted in a significant suppression of fluorescence emission (74%) (figure 4(b)). This phenomenon can be attributed to the nanoparticulate structure, which offers a different local environment to the bound ICG molecule when compared with the free form [33]. ICG molecules that are in close proximity within the nanoparticle assembly quench each another and this inevitably results in reduced fluorescence emission [34, 35]. As stated above, the fluorescence of free ICG gradually decreased overtime and 63% of the fluorescence is lost after 24 h of incubation. In the case of the system that was incubated in the presence of cathepsin B, fluorescence increased by 74% after 24 h, and at that point the intensity of the digested system was 77% higher than that of the free ICG, while fluorescence of the undigested nanoparticles remained low. This phenomenon confirms enzyme-induced nanoparticle degradation and increased ICG release during incubation, subsequently leading to fluorescence recovery. After 3 d incubation, fluorescence emission of the system under digestion decreased by 25% from day 1; however, intensity still remained 66% higher than that of free ICG.

Results on the absorbance and fluorescence emission profiles of the formulation, in comparison to those of free ICG, suggest that the assembly of the PGA nanoparticulate structure offers unique optical properties that can be exploited for improving the therapeutic efficacy of ICG as a tumour-specific photo-responsive agent, as well as for reinforcing the potential of this agent for applications in cancer diagnosis and imaging. As discussed, ICG is a promising NIR dye for tumour imaging; however, the poor stability, biodistribution and lack of targeting limit its application [24]. In this study, a nanoparticulate system has been designed for carrying ICG and with the intention of improving the biodistribution, tumour accumulation and stability profile of this agent. Moreover, the cathepsin B—induced increase in fluorescence emission observed at 24 h post-incubation of the nanoparticles demonstrates the potential of this formulation from a diagnostic perspective for the selective detection and imaging/delineation of highly aggressive tumours with elevated proteolytic enzyme activity.

3.3. Cellular uptake of nanoparticles

The cellular uptake of the ICG-containing nanoparticles (ICGNP) was examined and compared to the uptake of the ICG-containing PGA-nanoparticles that were digested with cathepsin B for three days (d.ICGNP). Cellular uptake of these formulations was also compared to that of free ICG, at the same concentration. In later part of this study, the efficacy of ICGNP in promoting endo/lysosomal escape of saporin is examined. For this reason, it was considered necessary to investigate the effect of saporin on nanoparticle cellular uptake, for more informative evaluation of the combined treatment. Results shown in figure 5(a) demonstrate that the use of PGA-based nanoparticles significantly improved cellular uptake of ICG by 3.2-fold ($p < 0.001$) in comparison to uptake of free ICG. In addition, uptake was further increased by 9% ($p < 0.05$) when the nanoparticles were digested with cathepsin-B. Interestingly, saporin facilitated a 42% increase in the uptake of ICG using the ICGNP system. This

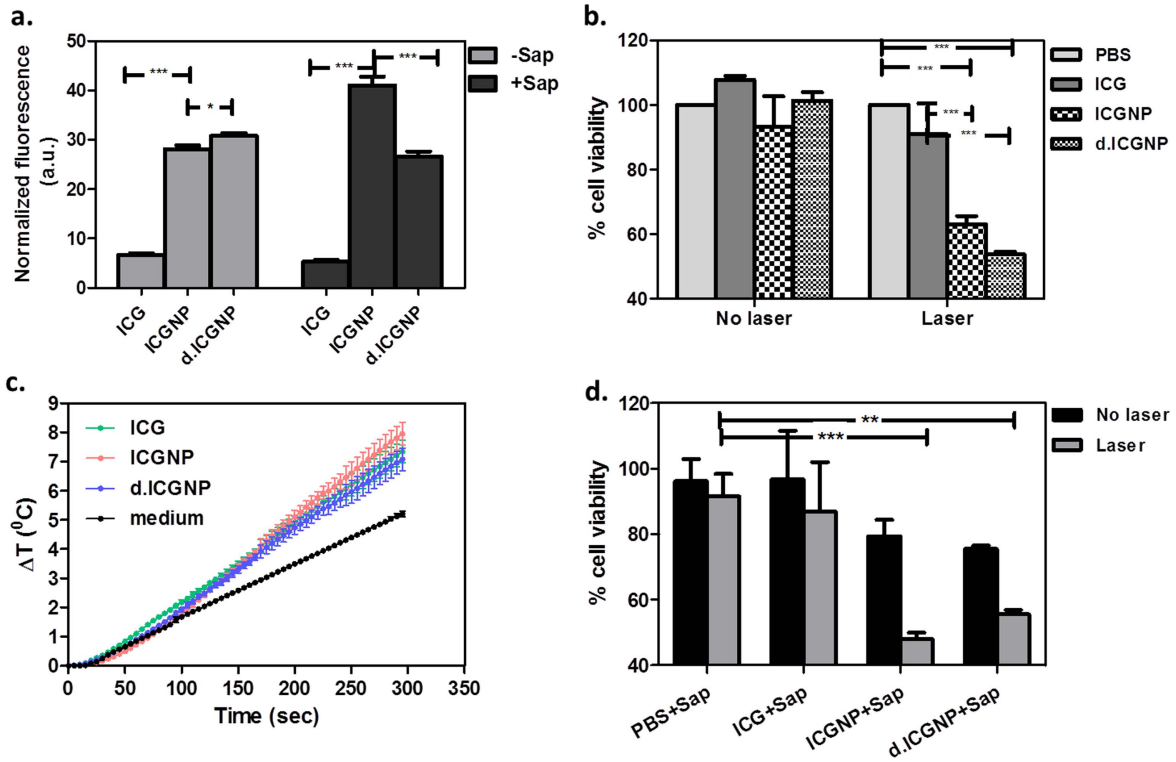

Figure 5. (a) Cellular uptake of ICG, ICGNP and d.ICGNP, in the absence (-Sap) or the presence (+Sap) of saporin. Data groups were compared using one-way ANOVA with Tukey's multiple comparison test (MCT) ($n = 3$). (b) Cell viability of SCC-9 cells treated with no ICG (PBS), ICG, ICGNP and d.ICGNP, under no laser irradiation or under NIR laser irradiation (805 nm, 150 mW cm^{-2}, 5 min) ($n = 3$). (c) Temperature profiles of laser-irradiated DMEM/Ham's F-12 (medium), ICG-containing medium, ICGNP-containing medium and d.ICGNP -containing medium ($n = 3$). (d) Cell viability of SCC-9 cells treated with no ICG (PBS), ICG, ICGNP and d.ICGNP in the presence of saporin (Sap), with no laser irradiation or under NIR laser irradiation (805 nm, 150 mW cm^{-2}, 5 min) ($n = 3$).

phenomenon can be explained by the fact that saporin is highly positively charged [36] and its electrostatic interaction with the cell membrane may enhance endocytic activity that concurrently increases cellular uptake of the negatively-charged nanoparticles. However, the cellular uptake of d. ICGNP was decreased by 13% ($p < 0.001$) in the presence of saporin. The latter can be attributed to the high protein affinity of free ICG released following nanoparticle degradation that could have inhibited efficient cellular uptake. Nevertheless, cellular uptake for both ICGNP and d.ICGNP in the presence of saporin was still significantly higher than the uptake using free ICG ($p < 0.001$).

It has been suggested that nanoparticles with sizes that are optimal for delivery on the basis of the EPR effect (20–200 nm) have poor diffusion within solid tumours following extravazation [37, 38]. In addition, smaller particles (<10 nm), with better tumour diffusion capability [39], are readily eliminated from blood circulation and show inefficient EPR-based delivery [40, 41]. The formulation described in this study has an appropriate size for increasing tumour accumulation through the EPR effect after administration via blood circulation. The innovative aspect of this formulation is that, upon degradation by cathepsin B, smaller particles are produced, which can potentially diffuse through the mass of dense tumour tissue more efficiently than the formulation that was initially administered. Moreover, according to the results in this study, degradation into smaller particles results in improved cellular uptake, further demonstrating the multi-dimensional benefit of this system.

MMP-mediated, site-specific drug delivery based on the chemical conjugation of drugs to either synthetic polymers or proteins that are recognized and cleaved by MMPs for release are currently under development [7, 42–44]. One disadvantage of this general approach is that the released drugs will have a peptide sequence or a residual part thereof attached, which can potentially compromise the activity of the drug. The formulation proposed in this study, presents an alternative approach to form a safe, stable and MMP-cleavable carrier, which does not necessitate any chemical modification of the payload.

3.4. NIR-laser treatment of cells

In order to examine the photo-induced effect of ICG-carrying nanoparticles on SCC-9 cells, the latter were treated with 45 J cm^{-2} total energy using 805 nm laser light following a 24 h incubation with the ICG formulations. The data shown in figure 5(b) demonstrate that incubation with free ICG and ICG-containing nanoparticles, either undigested or digested with cathepsin B, resulted in minimal toxicity without laser irradiation. Treatment with laser light resulted in 9%, 37% and 47% toxicity in the case of free ICG, ICGNP and d. ICGNP, respectively. These results demonstrate that incorporation of ICG in the PGA-based nanoparticles significantly

increased the effect of the agent under laser light exposure and this effect was primarily a result of the improved cellular uptake of the ICGNP and d.ICGNP formulations (figure 5(a)).

In the literature, a number of different mechanisms for the cytotoxic effect of ICG upon NIR irradiation have been suggested. Although the main mechanism has been described as a photothermal effect causing heat-mediated cell death, mechanisms such as the induction of mitochondrial dysfunction and the generation of cytotoxic singlet oxygen, possibly resulting from highly localized elevated temperatures, have also been suggested to be responsible for the effect of irradiated ICG on cells [22]. In our study, the ICG-dependent increase in temperature measured was in the range of 2 °C for all tested ICG forms (figure 5(c)). Although a low ICG-dependent increase in temperature was observed for the current system upon laser treatment, highly localized thermal effects at a microscopic level could be possible, particularly after ICG-nanoparticles from the incubation medium were concentrated in the subcellular environment (figure 5(a)). Previously, both studies by Wan *et al* [25], for A549 cells, and by Jian *et al* [45], for HeLa cells, showed a 25% cytotoxic effect using ICG-containing micelles, at equivalent ICG concentrations, upon irradiation with total energy of 270 J cm^{-2} and 375 J cm^{-2}, respectively. Herein, with significantly lower energy provided, the nanoparticles resulted in a 37% decrease in cell viability and nanoparticle digestion by cathepsin B contributed to an additional 10% in cell toxicity upon NIR treatment. Although, differences in the response to treatment among different cell lines do exist, these results demonstrate the improved performance of the proposed formulation in potentiating the NIR-triggered effect of ICG for anticancer therapy.

The tumour microenvironments in different human cancers have been extensively characterized, and most of them share the same characteristics, particularly at their advanced stages [1]. Specifically for oral squamous cell carcinoma, overexpression of cathepsin B has been correlated with carcinoma invasion and progression, and the level of expression of this protease has been studied as a prognostic indicator in patients with oral cancer [46]. In addition, when the EPR effect in oral cancer was exploited for NIR fluorescence optical imaging in preclinical studies, the tumours were clearly demarcated *in vivo* and confirmed by histological analysis to provide tumour-to-background ratios similar to those delivered using conventional contrast agents [47]. The afore-mentioned, in combination with their superficial nature, suggests that oral tumours present a suitable target for the proposed system.

3.5. Effect of nanoparticles on saporin toxicity

In order to study the effect of NIR-irradiated ICG nanoparticles on saporin toxicity, SCC-9 cells were co-incubated for 24 h with each ICG formulation and saporin at non-lethal doses. After washing with agent-free medium, cells were treated with laser light at the afore-mentioned parameters. Data shown in figure 5(d) demonstrate that, without laser irradiation, saporin had little effect on cell viability both in the presence and the absence of free ICG (PBS). Following laser light exposure, the mean cell viability decreased by 4% and 10% in the absence and the presence of free ICG, respectively. In the presence of nanoparticles, saporin toxicity without light irradiation was 21% and 25% ($p > 0.05$) in the case of the ICGNP and the d.ICGNP formulation, respectively. This phenomenon could suggest that the PGA-based nanoparticles interact with saporin and they either enhance cellular uptake of saporin and/or protect saporin from deactivation resulting from lysosomal enzyme degradation. Exposure to laser light resulted in significant cell toxicity when the combination of ICG nanoparticles and saporin was employed. In the presence of the ICGNP and d.ICGNP systems mean cell toxicity was increased to 52% and 45%, respectively. Comparison of these results with those in figure 5(b), where cells were irradiated in the presence of the ICG-containing nanoparticles, leads to the conclusion that even though a large proportion of cell toxicity in targets treated with saporin is attributed to the photo-induced toxicity of ICG-nanoparticles, a synergistic effect was observed with combined treatment. More specifically, in the case of the ICGNP, mean cell viability with light exposure was 63% and 48% in the absence and the presence of saporin, respectively. Taking into consideration the 4% toxicity caused by saporin alone under light irradiation, a synergistic effect of 11% in cell toxicity was found. From a similar perspective, the results did not demonstrate that there was a synergistic effect in the case of the d.ICGNP formulation suggesting that the intact nanoparticles are playing some role in enhancing the toxicity of saporin.

The synergistic effect of ICGNP and saporin on toxicity with laser light exposure was attributed to the photo-induced drug internalization effect of the nanoparticles. In order to further investigate this hypothesis, rhodamine-dextran was employed as a surrogate for saporin in order to examine the influence of the ICGNPs on its intracellular localization/distribution using fluorescence microscopy. SCC-9 cells were co-incubated with rhodamine-dextran, in the presence or the absence of ICGNP for 24 h. Cells were washed, treated with laser light at the conditions described above and stained with LysoTracker® Green. Figure 6 illustrates the photo-induced effect of the ICGNP on lysosomal release of rhodamine-dextran. In the absence of ICG-nanoparticles (panel A) the fluorescence of LysoTracker and rhodamine-dextran were co-localized, implying that the latter was mainly localized in the endo/lysosomal compartments. After laser irradiation in the presence of ICGNP and d.ICGNP (panels B and C), rhodamine-dextran appeared to disperse throughout the cytosol when compared with the green fluorescence emanated from stained endo/lysosomes. Image analysis for red (rhodamine) pixels along representative cytoplasmic regions demonstrated that in the systems irradiated in the absence of nanoparticles, the lysosomal localization of rhodamine-dextran in the cytoplasm is demonstrated by isolated peaks in figure 7(b), while the systems treated in the presence of ICGNP and d.ICGNP display dense peak profiles that demonstrate diffused cytoplasmic distribution of rhodamine. These observations demonstrated the successful ICGNP-mediated, photo-induced

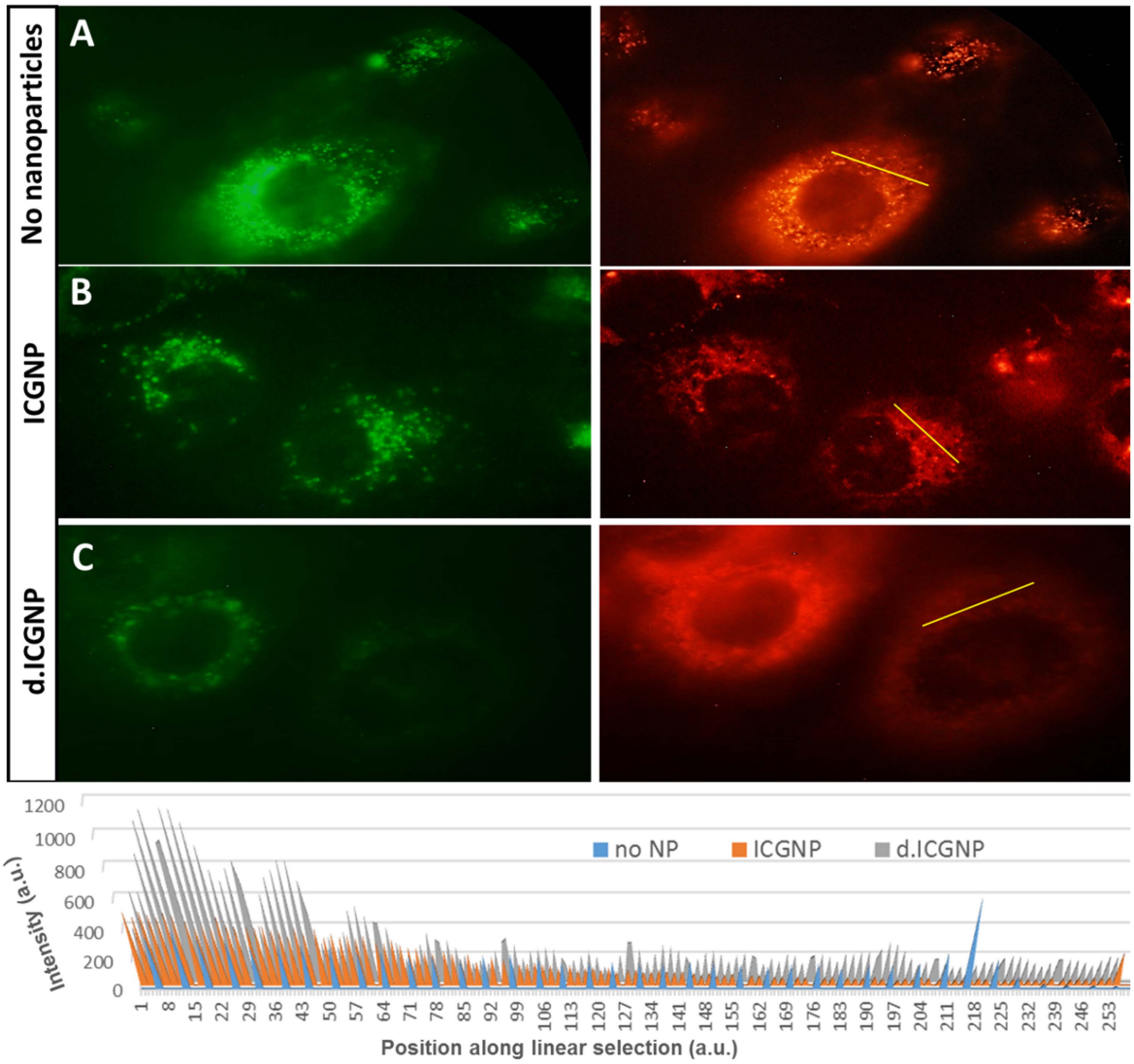

Figure 6. NIR laser-induced release of rhodamine-dextran in SCC-9 cells: (a) fluorescence images of cells in the absence of ICG-containing nanoparticles (No NP) (panel A), the presence of ICGNP (panel B) and the presence of d.ICGNP (panel C). Systems were irradiated with NIR at 805 nm, 150 mW cm^{-2}, for 5 min Endo/lysosomes were stained with green Lysotracker (left panels) and red was the fluorescence of rhodamine-dextran (right panels). (b) Image analysis for red (rhodamine) pixels along linear selection (yellow line) of representative cytoplasmic regions.

endo/lysosomal escape of rhodamine-dextran and its diffusion in the cytosol. Previous reports have demonstrated photothermally-induced toxicity and endo/lysosomal escape of drugs using graphene oxide,or non-biodegradable iron oxide and silver nanoparticles [15, 48–50]. In the current study, a biodegradable, tumour-responsive formulation has been developed that, at sub-lethal concentrations and under significantly lower irradiation energy densities, offers a similar attribute demonstrated by the induction of cellular internalization and endo/lysosomal release of large molecules. In the absence of the photo-induced internalization effect elicited here by NIR in combination with the ICGNPs, saporin is ineffective because its target is intracellular and, as mentioned, it is membrane impermeable. Saporin molecules that would be internalized into the cell would gain access by an endocytotic route and remain within the endo/lysosomes until eradicated within those vesicles by proteolysis. The aspect of synergistically enhancing chemotherapy, in combination with the proto-induced cytotoxic effect of the formulation, reveals the dual effect of the latter in NIR-based tumour treatment and signifies its potential applicability for the management of head and neck or other superficial cancers.

ICG has previously been described as a trifunctional agent for photothermal therapy, as photothermal agent for hyperthermia-triggered drug release and for optical imaging. In a similar study, ICG-containing nano-liposomes were developed for intratumoral release of doxorubicin with laser light at 808 nm [16]. When irradiated with light of energy that was more than three-fold higher than the energy provided in the current treatment, the system exhibited synergistic cytotoxic effects only at elevated doxorubicin concentrations, where dark toxicity was higher than 70%. For the system developed in this study, dark toxicity did not exceed 25%, even in the presence of saporin. Low dark toxicity is

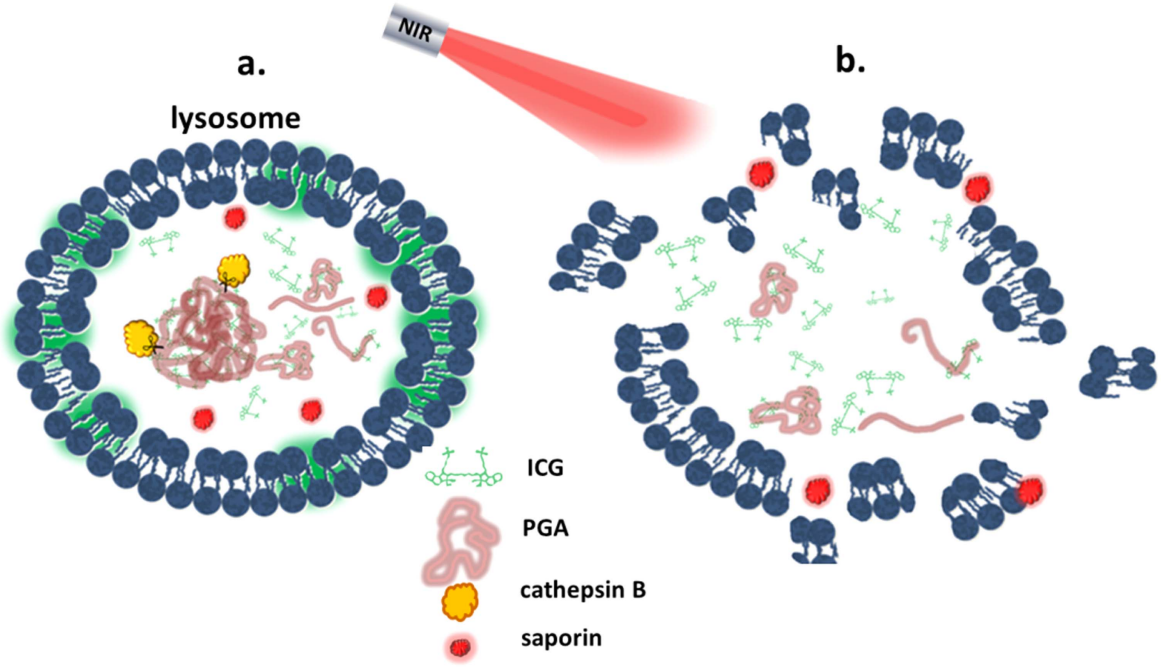

Figure 7. (a) Endo-lysosomal membrane sensitization with ICG released from enzymatic digestion of nanoparticles, and (b) NIR laser-induced endo/lysosome disruption and subsequent escape of the endocytosed saporin.

particularly important for the clinical translation of a photothermal ablative approach, in order to avoid post-treatment, off-target cytotoxic effects and skin irritation.

The amphiphilic nature of ICG makes it suitable for sensitizing endo/lysosomal membranes. For membrane sensitization, release of free ICG from the PGA-based formulation can occur in the tumour extracellular environment by the action of cell-excreted cathepsin B or inside the lysosome by the action of lysosomal cathepsin B (figure 7). Extracellular ICG release can result in sensitization of the lysosome following its fusion with the endosome, which is part of the cytoplasmic membrane that carries ICG. Nanoparticle degradation inside the lysosome releases ICG that can directly sensitize the lysosomal membrane. In the case of PCI treatment for enhancing chemotherapy, it has been suggested that sensitizer-induced lysosomal rupture upon light irradiation results from free radical-mediated lipid peroxidation and subsequent membrane destabilization [51]. As an NIR fluorophore, ICG has significantly lower quantum yield (approx. 4.3% quantum yield at the emission wavelength of 805 nm) than organic molecules with shorter emission wavelengths in the visible region of the electromagnetic spectrum [52]. Despite the latter, it has previously been demonstrated that excitation of ICG with light at 805 nm can cause a Type II photodynamic reaction resulting in the generation of singlet oxygen and the subsequent generation of lipid peroxides followed by cell death [20]. Wan *et al* showed that low concentrations of ICG ($<2\,\mu g\,ml^{-1}$) can deliver a weak photo-induced hyperthermic effect [25]. They suggested that the synergistic cytotoxicity induced by ICG at these low concentrations, when used together with doxorubicin co-harboured in micelles, is unlikely to have originated from hyperthermia. Instead, it was hypothesized that the synergistic cytotoxicity was correlated with the generation of intracellular singlet oxygen from the amphiphilic ICG, which triggered the disruption of the lysosomal membranes via a PCI effect (figure 7), and subsequently induced enhanced susceptibility of cancer cells to the chemotherapeutic agent [51].

4. Conclusion

Here, a formulation with dual responsiveness to both a tumour-specific and an external stimulus was developed and characterized. The nanoparticulate nature of the formulation has the potential to facilitate improved tumour-accumulation capability of an otherwise poorly-biodistributed photothermal agent. Incubation with cathepsin B decreased nanoparticle size and contributed to time-dependent ICG release. The results clearly demonstrated that nanoparticle degradation by cathepsin B can further increase cellular uptake and subsequent photo-induced toxicity under NIR laser irradiation. The formulation used in this study exhibited a photo-induced drug internalization effect, when it was tested in combination with the otherwise cell membrane-impermeable saporin. Saporin contributed to increased cytotoxicity of this treatment approach in a synergistic manner using the ICG-containing nanoparticles. Fluorescence microscopy using rhodamine-dextran as a saporin surrogate suggested that the synergistic effect was due to photo-induced drug internalization following sensitization and light-induced disruption of the endo/lysosomal membrane in the presence of the ICG-containing nanoparticles.

The main objectives of this study were to establish the properties of the PGA-based formulation containing an NIR-based agent, investigate its response to light irradiation and

cathepsin B, and correlate this response to subsequent cell cytotoxicity. The treatment based on the ICG-containing formulation described here has been designed to be used in combination with any cytotoxic agent, particularly large biomolecules such as saporin or membrane impermeable chemotherapeutic agents such as bleomycin that can only enter cells via endocytosis and may be susceptible to deactivation by lysosomal enzymes and acidic pH. It is reasonable to anticipate that the performance of the combined treatment proposed here can be improved by co-harbouring the cytotoxic agent and ICG in the PGA-based nanoparticles. Importantly, future studies that will focus on the drug-internalization aspect of the formulation, will employ PGA-nanoparticles that co-harbour the photoresponsive and cytotoxic agents. Future studies will also aim to characterize the performance of the proposed formulation in experimental animal models for the treatment of orthotopic head and neck tumours. Aspects, such as tumour accumulation, pharmacokinetic profiles, diffusion throughout the tumour mass, photothermal antitumour efficacy, the potential to enhance chemotherapy and the level of spatial control of the treatment itself, will be examined. In addition, considering the clinically established acceptability of ICG as an imaging agent, the diagnostic role of the proposed formulation will also be evaluated for simultaneous tumour delineation, as a reporter of payload release/nanoparticle degradation and precise locoregional deposition. This diagnostic feature will further emphasize the multifunctional potential of the formulation described here in cancer therapy.

Acknowledgments

The authors would like to thank the Royal Society UK (First Grant Scheme, RG130569) for financially supporting part of this work.

References

[1] Du J, Lane L A and Nie S 2015 Stimuli-responsive nanoparticles for targeting the tumor microenvironment *J. Control. Release* **219** 205–14
[2] Webb B A, Chimenti M, Jacobson M P and Barber D L 2011 Dysregulated pH: a perfect storm for cancer progression *Nat. Rev. Cancer* **11** 671–7
[3] Maeda H, Nakamura H and Fang J 2013 The EPR effect for macromolecular drug delivery to solid tumors: improvement of tumor uptake, lowering of systemic toxicity, and distinct tumor imaging *in vivo Adv. Drug. Deliv. Rev.* **65** 71–9
[4] de la Rica R, Aili D and Stevens M M 2012 Enzyme-responsive nanoparticles for drug release and diagnostics *Adv. Drug. Deliv. Rev.* **64** 967–78
[5] Brown J M and Wilson W R 2004 Exploiting tumour hypoxia in cancer treatment *Nat. Rev. Cancer* **4** 437–47
[6] Akhtar M J, Ahamed M, Alhadlaq H A, Alrokayan S A and Kumar S 2014 Targeted anticancer therapy: overexpressed receptors and nanotechnology *Clin. Chim. Acta* **436** 78–92
[7] Chipman S D, Oldham F B, Pezzoni G and Singer J W 2006 Biological and clinical characterization of paclitaxel poliglumex (PPX, CT-2103), a macromolecular polymer-drug conjugate *Int. J. Nanomedicine* **1** 375–83
[8] Roshy S, Sloane B F and Moin K 2003 Pericellular cathepsin B and malignant progression *Cancer Metastasis Rev.* **22** 271–86
[9] Li C *et al* 2000 Biodistribution of paclitaxel and poly(L-glutamic acid)-paclitaxel conjugate in mice with ovarian OCa-1 tumor *Cancer Chemotherapy Pharmacology* **46** 416–22
[10] Homsi J *et al* 2007 Phase I trial of poly-L-glutamate camptothecin (CT-2106) administered weekly in patients with advanced solid malignancies *Clin. Cancer Res.* **13** 5855–61
[11] Singer J W *et al* 2005 Paclitaxel poliglumex (XYOTAX; CT-2103): an intracellularly targeted taxane *Anticancer Drugs* **16** 243–54
[12] Dolmans D E, Fukumura D and Jain R K 2003 Photodynamic therapy for cancer *Nat. Rev. Cancer* **3** 380–7
[13] Andrzejak M, Santiago M and Kessel D 2011 Effects of endosomal photodamage on membrane recycling and endocytosis *Photochem. Photobiol.* **87** 699–706
[14] Norum O J, Selbo P K, Weyergang A, Giercksky K E and Berg K 2009 Photochemical internalization (PCI) in cancer therapy: from bench towards bedside medicine *J. Photochem. Photobiol.* B **96** 83–92
[15] Kim H, Lee D, Kim J, Kim T I and Kim W J 2013 Photothermally triggered cytosolic drug delivery via endosome disruption using a functionalized reduced graphene oxide *ACS Nano* **7** 6735–46
[16] Zhao P *et al* 2015 NIR-driven smart theranostic nanomedicine for on-demand drug release and synergistic antitumour therapy *Sci. Rep.* **5** 14258
[17] Weissleder R 2001 A clearer vision for *in vivo* imaging *Nat. Biotechnol.* **19** 316–7
[18] Gazouli M, Nomikou N, Callan J F and Efstathopoulos E P 2016 Novel nanotechnology approaches for targeted cancer therapy *Curr. Nanomed.* **3** 83–8
[19] Baumler W *et al* 1999 Photo-oxidative killing of human colonic cancer cells using indocyanine green and infrared light *Br. J. Cancer* **80** 360–3
[20] Yan L and Qiu L 2015 Indocyanine green targeted micelles with improved stability for near-infrared image-guided photothermal tumor therapy *Nanomedicine (Lond)* **10** 361–73
[21] Nomikou N, Sterrett C, Arthur C, McCaughan B, Callan J F and McHale A P 2012 The effects of ultrasound and light on indocyanine-green-treated tumour cells and tissues *ChemMedChem* **7** 1465–71
[22] Ott P 1998 Hepatic elimination of indocyanine green with special reference to distribution kinetics and the influence of plasma protein binding *Pharmacol Toxicol* **83** 1–48
[23] Zheng X, Xing D, Zhou F, Wu B and Chen W R 2011 Indocyanine green-containing nanostructure as near infrared dual-functional targeting probes for optical imaging and photothermal therapy *Mol. Pharm.* **8** 447–56
[24] Zheng M *et al* 2013 Single-step assembly of DOX/ICG loaded lipid–polymer nanoparticles for highly effective chemo-photothermal combination therapy *ACS Nano* **7** 2056–67
[25] Wan Z *et al* 2014 Highly efficient hierarchical micelles integrating photothermal therapy and singlet oxygen-synergized chemotherapy for cancer eradication *Theranostics* **4** 399–411
[26] Yamaguchi F, Ogawa Y, Kikuchi M, Yuasa K and Motai H 1996 Detection of gamma-polyglutamic acid (gamma-PGA) by SDS-Page *Biosci. Biotechnol. Biochem.* **60** 255–8
[27] Zia Q, Khan A A, Swaleha Z and Owais M 2015 Self-assembled amphotericin B-loaded polyglutamic acid nanoparticles: preparation, characterization and *in vitro*

potential against Candida albicans *Int. J. Nanomedicine* **10** 1769–90
[28] Beziere N, Lozano N, Nunes A, Salichs J, Queiros D, Kostarelos K and Ntziachristos V 2015 Dynamic imaging of PEGylated indocyanine green (ICG) liposomes within the tumor microenvironment using multi-spectral optoacoustic tomography (MSOT) *Biomater.* **37** 415–24
[29] Rajian J R, Fabiilli M L, Fowlkes J B, Carson P L and Wang X 2011 Drug delivery monitoring by photoacoustic tomography with an ICG encapsulated double emulsion *Opt. Express* **19** 14335–47
[30] Weigand R, Rotermund F and Penzkofer A 1997 Aggregation dependent absorption reduction of indocyanine green *J. Phys. Chem.* A **101** 7729–34
[31] Awasthi K and Nishimura G 2011 Modification of near-infrared cyanine dyes by serum albumin protein *Photochem. Photobiol. Sci.* **10** 461–3
[32] Kirchherr A K, Briel A and Mader K 2009 Stabilization of indocyanine green by encapsulation within micellar systems *Mol. Pharm.* **6** 480–91
[33] Ng K K and Zheng G 2015 Molecular interactions in organic nanoparticles for phototheranostic applications *Chem. Rev.* **115** 11012–42
[34] Mordon S, Devoisselle J M, Soulie-Begu S and Desmettre T 1998 Indocyanine green: physicochemical factors affecting its fluorescence *in vivo Microvasc. Res.* **55** 146–52
[35] Kelkar S S, Hill T K, Marini F C and Mohs A M 2016 Near infrared fluorescent nanoparticles based on hyaluronic acid: self-assembly, optical properties, and cell interaction *Acta Biomater.* **36** 112–21
[36] Weng A *et al* 2015 Improved intracellular delivery of peptide- and lipid-nanoplexes by natural glycosides *J. Control. Release* **206** 75–90
[37] Allen T M and Cullis P R 2004 Drug delivery systems: entering the mainstream *Science* **303** 1818–22
[38] Cabral H *et al* 2011 Accumulation of sub-100 nm polymeric micelles in poorly permeable tumours depends on size *Nat. Nanotechnol.* **6** 815–23
[39] Wong C *et al* 2011 Multistage nanoparticle delivery system for deep penetration into tumor tissue *Proc. Natl Acad. Sci. USA* **108** 2426–31
[40] Choi H S *et al* 2010 Design considerations for tumour-targeted nanoparticles *Nat. Nanotechnol.* **5** 42–7
[41] Choi H S *et al* 2007 Renal clearance of quantum dots *Nat. Biotechnol.* **25** 1165–70
[42] Mansour A M *et al* 2003 A new approach for the treatment of malignant melanoma: enhanced antitumor efficacy of an albumin-binding doxorubicin prodrug that is cleaved by matrix metalloproteinase 2 *Cancer Res.* **63** 4062–6
[43] Lee G Y, Park K, Kim S Y and Byun Y 2007 MMPs-specific PEGylated peptide-DOX conjugate micelles that can contain free doxorubicin *Eur. J. Pharm. Biopharm.* **67** 646–54
[44] Chen W H *et al* 2015 MMP-2 responsive polymeric micelles for cancer-targeted intracellular drug delivery *Chem. Commun. (Camb)* **51** 465–8
[45] Jian W H, Yu T W, Chen C J, Huang W C, Chiu H C and Chiang W H 2015 Indocyanine green-encapsulated hybrid polymeric nanomicelles for photothermal cancer therapy *Langmuir* **31** 6202–10
[46] Kawasaki G, Kato Y and Mizuno A 2002 Cathepsin expression in oral squamous cell carcinoma: relationship with clinicopathologic factors *Oral Surg. Oral Med. Oral Pathol. Oral Radiol. Endod.* **93** 446–54
[47] Keereweer S *et al* 2012 Targeting integrins and enhanced permeability and retention (EPR) effect for optical imaging of oral cancer *J. Surg. Oncol.* **105** 714–8
[48] Ochs M, Carregal-Romero S, Rejman J, Braeckmans K, De Smedt S C and Parak W J 2013 Light-addressable capsules as caged compound matrix for controlled triggering of cytosolic reactions *Angew. Chem., Int. Ed. Engl.* **52** 695–9
[49] Zhu B, Li Y, Lin Z, Zhao M, Xu T, Wang C and Deng N 2016 Silver nanoparticles induce HePG-2 cells apoptosis through ROS-mediated signaling pathways *Nanoscale Res. Lett.* **11** 198
[50] Zhang Z, Wang J and Chen C 2013 Near-Infrared light-mediated nanoplatforms for cancer thermo-chemotherapy and optical imaging *Adv. Mater.* **25** 3869–80
[51] Berg K *et al* 1999 Photochemical internalization: a novel technology for delivery of macromolecules into cytosol *Cancer Res.* **59** 1180–3
[52] Philip R, Penzkofer A, Bäumler W, Szeimies R M and Abels C 1996 Absorption and fluorescence spectroscopic investigation of indocyanine green *J. Photochem. Photobiol. A Chem.* **96** 137–48